



OPEN

Synthesis of $\text{Cu}_x\text{O}/\text{Ag}$ nanoparticles on exfoliated graphene: application for enhanced electrochemical detection of H_2O_2 in milk

Jie Song¹, Yating Wan¹, Chen Yang¹, Qiuju Deng¹, Yingde Cui^{4✉}, Zhihong Yan^{2✉} & Yi Liu^{1,2,3✉}

In this paper, a novel composite is constructed as a non-enzymatic hydrogen peroxide (H_2O_2) sensor by liquid-phase exfoliation method, which is composed of copper oxide, cuprous oxide and silver nanoparticles doped few-layer-graphene ($\text{Cu}_x\text{O}/\text{Ag}@\text{FLG}$). Its surface morphology and composition were characterized by scanning electron microscopy (SEM) and X-ray photo spectroscopy (XPS), and its H_2O_2 sensing performances include catalytic reduction and quantitative detection were studied with electrochemical methods. Our sensor had a high sensitivity of $174.5 \mu\text{A mM}^{-1} \text{cm}^{-2}$ ($R^2 = 0.9978$) in an extremely wide range of concentrations from $10 \mu\text{M}$ to 100mM , a fast response (about 5 s) and a low limit of detection ($S/N = 3$) of $2.13 \mu\text{M}$. The sensor exhibits outstanding selectivity in the presence of various biological interference, such as dopamine, ascorbic acid, uric acid, citric acid, etc. In addition, the constructed sensor continued 95% current responsiveness after 1 month of storage further points to its long-term stability. Last but not least, it has a good recovery rate (90.12–102.00%) in milk sold on the open market, indicating that it has broad application possibilities in the food industry and biological medicine.

H_2O_2 is commonly used as a bleaching agent, disinfectant, and preservative in the food industry, owing to its strong oxidation resistance, good antibacterial and bactericidal properties¹. H_2O_2 is not only one of the by-products of many classical enzymatic reactions, such as glucose oxidation, uric acid oxidation, oxalic acid oxidation, amino acid oxidation, glutamic acid, lysine oxidation, etc.², but also plays a significant role as the primary messenger molecule in the cellular and redox metabolism³. It is worth noting that H_2O_2 has strong oxidizability, ingesting residual H_2O_2 in food will consume antioxidant substances in the body, accelerate the aging process of the human body, and reduce the resistance after ingestion. Excessive H_2O_2 in the body will produce a large number of $\text{OH}\cdot$, which participates electron transfer and hydroxylation reaction in biochemical process, damage cells, induce gene mutation and various diseases, even cause human cell canceration⁴. In 2017, the list of carcinogens was announced by International Agency for Research on Cancer of the World Health Organization, and H_2O_2 appeared in the list of Class III carcinogens⁵. At present, it has been detected in the market that excessive amounts of H_2O_2 residues exist in prepackaged milk, beverages, soy products, aquatic products, chicken feet, etc., posing a serious threat to human health. Therefore, the newly revised National Food Safety Standard in China (GB 2760-2014) stipulates that H_2O_2 can be used as a food processing aid in various food processing processes, and the residual amount does not need to be limited, but it needs to be removed from the finished product. The Food and Drug Administration (FDA) requires H_2O_2 to be used as an antimicrobial agent in milk, with a residual amount not exceeding 0.05 wt% in 21 CFR 184.1366. In addition, it is also stipulated that H_2O_2 solution should be used in the sterilization of food packaging materials, and the residual amount of H_2O_2 in distilled water after packaging should be less than 0.5 parts per million (testing should be conducted immediately after packaging) in 21 CFR 178.1005. Therefore, sensitive detection of H_2O_2 is crucial for monitoring the quality of food and for applications of clinical, and biomedical.

¹School of Pharmaceutical and Chemical Engineering, Guangdong Pharmaceutical University, Zhongshan 528400, China. ²College of Pharmacy, Guangdong Pharmaceutical University, Guangzhou 510000, China. ³Guangdong Provincial Key Laboratory of Advanced Drug Delivery Systems and Guangdong Provincial Engineering Center of Topical Precise Drug Delivery System, The Center for Drug Research and Development, Guangdong Pharmaceutical University, Guangzhou 510006, Guangdong, China. ⁴Guangzhou Vocational University of Science and Technology, Guangzhou 510555, China. ✉email: 13602880087@139.com; yzhxsp@aliyun.com; Liuyi915@126.com

Nowadays, the methods used in the detection of H_2O_2 include titration, spectroscopy, chromatography, chemiluminescence and electrochemical methods⁶. The Chinese national standard GB 5009. 226-2016 stipulates that the determination methods for H_2O_2 in food residues are iodometry and titanium salt colorimetry. The quantitative limit of the above two methods is 3 mg kg^{-1} . These two methods are cumbersome, time-consuming, poor selectivity, and low accuracy, making it difficult to achieve trace detection. However, electrochemical method has the advantages of rapid response, rapid response, high-cost efficiency, simple operation, high selectivity and high sensitivity⁷. The first generation electrochemical H_2O_2 detector relies on the reaction of enzyme with hydrogen peroxide. This enzyme-based technology has been mature and can now provide high sensitivity, high selectivity and low background noise⁸. Nevertheless, the complex process of immobilizing the enzyme on the electrode, strict conditions to maintain the enzyme activity, and the lack of long-term stability and reproducibility limit the application of this technology. More importantly, almost all enzymes are made of proteins, which will hinder the electrochemical reaction on the surface of electrode⁹. Therefore, non-enzymatic electrochemical H_2O_2 detection have been developed to eliminate these shortcomings due to its faster and more effective electron transport¹⁰.

Enzyme-free H_2O_2 sensors generally prepared by precious metal nanoparticles (NPs) include Au, Ag, Pt and Pd NPs¹¹. As a precious metal, Ag NPs have large specific surface area, good stability, good biocompatibility, excellent conductivity and electrocatalytic activity¹². It is reported that Tran et al. have successfully developed a series of electrochemical sensors based on AgNPs for sensitive detection for glucose and H_2O_2 ¹³⁻¹⁵. But expensive cost, poor tolerance immensely limits their mercantile application. Consequently, it is urgent to develop low-cost, reliable and sensitive H_2O_2 electrochemical sensing materials. So far, Co_3O_4 , Fe_3O_4 , Cu_2O , MnO_2 have been successfully applied in H_2O_2 electrochemical sensors¹⁶. CuO and Cu_2O have also been developed to prepare H_2O_2 sensors, which are inexpensive and strong stability, but with low sensitivity and narrow linear detection range. However, metal NPs have limited catalytic ability, because they are easily oxidized, and aggregative owing to the existence of van der Waals force between NPs¹⁷. In order to improve this problem, a suitable carrier is needed. At present, the substrates that have been widely studied are usually carbon materials, including ordered mesoporous carbon, carbon nanotubes, carbon nanofibers and graphene¹⁸. Among them, graphene has high specific surface area, good thermal stability, good conductivity, stability and high electron transfer ability, and its surface defects can anchor metal NPs, so it is an excellent carrier material¹⁹. Most of the existing related studies use graphene oxide prepared by Hummer's method as carbon substrate to prepare metal nanoparticle composites. The preparation process is complex, and the distribution position and size of metal particles are uneven, which affects the sensing performance of the composites²⁰. The liquid phase exfoliated method is low-cost, simple and controllable, green and environmentally friendly, and easy to large-scale production. It has been studied for use in Cd^{2+} and Pb^{2+} sensors, as well as flavomycin sensors^{20,21}.

In this work, we have used water-in-oil emulsion as a stabilizing system to synthesis $\text{Cu}_x\text{O}/\text{Ag}@/\text{FLG}$ composite by a simple ultrasonic exfoliation method for the first time. After a series of characterization, the morphology and structure of the composite were studied and modified on a glassy carbon electrode (GCE) to explore the detection of H_2O_2 performance. Compared with the reported Ag, CuO or Cu_2O NPs for H_2O_2 sensors, the $\text{Cu}_x\text{O}/\text{Ag}@/\text{FLG}/\text{GCE}$ H_2O_2 electrochemical sensor has the advantages of simple preparation, low cost and stable physicochemical properties. Our electrochemical experiments show the prepared sensor displays wide linear range, high sensitivity and selectivity toward the reduction of H_2O_2 with a low detection, and we also demonstrate it is successfully used to detect the concentration of H_2O_2 in milk. This study would offer a new routine for developing graphene-based electrochemical sensors for detecting H_2O_2 .

Experimental

Materials. Graphite was purchased from Sinopharm Chemical Reagent Co.,Ltd (Shanghai, China), Tween 80, $\text{NH}_3\cdot\text{H}_2\text{O}$ purchased from Shanghai Yien Chemical Technology Co., Ltd (Shanghai, China), cyclohexane were purchased from Guangzhou Chemical Reagent Factory (Guangzhou, China), Span 80 was purchased from Shanghai yuanye Bio-Technology Co., Ltd (Shanghai, China), ethanol, $\text{CuSO}_4\cdot 5\text{H}_2\text{O}$, AgNO_3 , NaBH_4 , NaCl , FeCl_3 , glucose (Glu) and CaCl_2 were purchased from Shanghai Aladdin Biochemical Technology Co., Ltd (Shanghai, China), MgCl_2 were purchased from Damao Chemical Reagent Factory (Tianjin, China), hydrogen peroxide(H_2O_2) was purchased from Jiangsu Qiangsheng functional Chemistry Co., Ltd (Jiangsu, China), Ltd (Beijing, China), glycine (Gly), lysine (Lys) were purchased from Nine-Dinn Chemistry Co., Ltd. (Shanghai, China), dopamine (DA), uric acid (UA), citric acid (CA), lactic acid (LA), arginine (Arg), valine (Val) were purchased from Shanghai McLean Biochemical Technology Co., Ltd (Shanghai, China), polyvinylpyrrolidone k30 (PVP k30) was purchased from Shanghai bide Pharmaceutical Technology Co., Ltd (Shanghai, China).

Synthesis of $\text{Cu}_x\text{O}/\text{Ag}@/\text{FLG}$ composite. 0.4 g graphite powder, 5 mL 3 wt% CuSO_4 in 2 wt% PVP solution, 3 g Tween 80, 4 g Span 80, 5 mL anhydrous ethanol are added into 30 mL cyclohexane, stable emulsion can be formed through vortex mixing. Then, ultrasonic unit is used to exfoliate the above solution for 2 h, with 40 kHz ultrasonic power. After that, 0.057 g NaBH_4 is added into the emulsion above and exfoliate the above solution for 2 h. Finally, the solid were carefully collected by filter to obtain $\text{Cu}_x\text{O}@/\text{FLG}$.

0.4 g $\text{Cu}_x\text{O}@/\text{FLG}$, 5 ml 3 wt% AgNO_3 in 2 wt% PVP and 20% $\text{NH}_3\cdot\text{H}_2\text{O}$ mixing solution, 3 g Tween 80, 4 g Span 80, 5 mL anhydrous ethanol are added into 30 mL cyclohexane, stable emulsion can be formed through vortex mixing. Then, ultrasonic cleaner is used to exfoliate the above solution for 2 h. At the end, the solid were carefully collected by filter to obtain $\text{Cu}_x\text{O}/\text{Ag}@/\text{FLG}$.

Fabrication of $\text{Cu}_x\text{O}/\text{Ag}@/\text{FLG}/\text{GCE}$ electrodes. Before modification, bare GCE was polished with $0.05 \mu\text{m}$ alumina powder and ultrasonically cleaned with ethanol and water for 5 min. $5 \mu\text{L}$ of 1 mg mL^{-1} of well-dispersed $\text{Cu}_x\text{O}/\text{Ag}@/\text{FLG}$ solution (include 0.05 wt% Chitosan and 0.5% acetic acid) was dropped to the washed

GCE and dried under an infrared drying lamp for 10 min to prepare $\text{Cu}_x\text{O}/\text{Ag}@/\text{FLG}/\text{GCE}$. For comparison, we prepared $\text{Cu}_x\text{O}@/\text{FLG}/\text{GCE}$ and $\text{Ag}@/\text{FLG}/\text{GCE}$ using the same method.

Analytical procedure. JSM-7610F PLUS scanning electron microscope (SEM, JEOL, Tokyo, Japan), H-7650 transmission electron microscope (TEM, Hitachi, Tokyo, Japan), D/max-2200/PC X-ray diffractometer (XRD, Hitachi, Tokyo, Japan) and ESCALAB 250 X-ray Photoelectron Spectroscopy (XPS, Thermo Fisher Scientific, Massachusetts, America) were used to characterize the surface morphology and structure. Cyclic Voltammetry (CV), electrochemical impedance spectroscopy (EIS) and Chronoamperometry ($i-t$) were determined by the CHI660E electrochemical workstation (CH Instruments, Shanghai, China). Electrolyte was consisting of phosphoric acid buffer solution, the working electrode was modified GCE, the counter electrode was platinum sheet, the reference electrode was saturated calomel electrode (SCE). The $i-t$ test was performed by adding H_2O_2 within a time interval of 40 s.

Results and discussion

Characterizations of morphology.

The construction and detection principles of the $\text{Cu}_x\text{O}/\text{Ag}@/\text{FLG}/\text{GCE}$ sensor are summarized in Fig. 1a. Next, the morphology of the material was characterized. The SEM image depicted in Fig. 1b shown that FLG with distinct crumples surface and large size were obtained, and there are lots of Ag nanoparticles and flower-like Cu_xO nanosheet supported on the surface of crumble layers of exfoliated graphene. Furthermore, EDS images shown in Fig. 1c confirm the existence and homogenous distribution of C, O, Cu, Ag elements. Two-dimensional conductive network structure has been developed in $\text{Cu}_x\text{O}/\text{Ag}@/\text{FLG}$, which is conducive to the rapid transfer and conduction of electrons, so as to detect target analytes sensitively.

As a supplement, the micromorphologies and microstructures of synthetic $\text{Cu}_x\text{O}/\text{Ag}@/\text{FLG}$ investigated by TEM. As shown in Fig. 2a,b, the metal NPs were successfully loaded on the graphene sheet. The lattice spacing in Fig. 2c was 0.343 nm, belonging to the (002) crystal plane of graphene (JCPDS no. 41-1487). Interplanar distances of 0.249 nm and 0.247 nm indexed to the (002) crystal plane of CuO (JCPDS no. 45-0937), interplanar distance of 0.219 nm belongs to the (200) crystal plane of Cu_2O (JCPDS no. 74-1230). The lattice spacing of 0.254 nm corresponds to the (111) crystal plane of Ag^0 (JCPDS no. 04-0783) (Fig. 2d,e). In addition, the Raman spectrum compares the graphite powder raw material with the prepared material, as shown in Fig. 2f and Table 1. The peak position of the G peak and 2D peak move to the low frequency direction, and the half peak width of 2D peak decreases, and the I_{2D}/I_G increases, which indicate the successful preparation of FLG²². Besides, the same trend as TEM images could be observed in XRD pattern. As can be seen from Fig. 2g, the strong peak at 26.38°

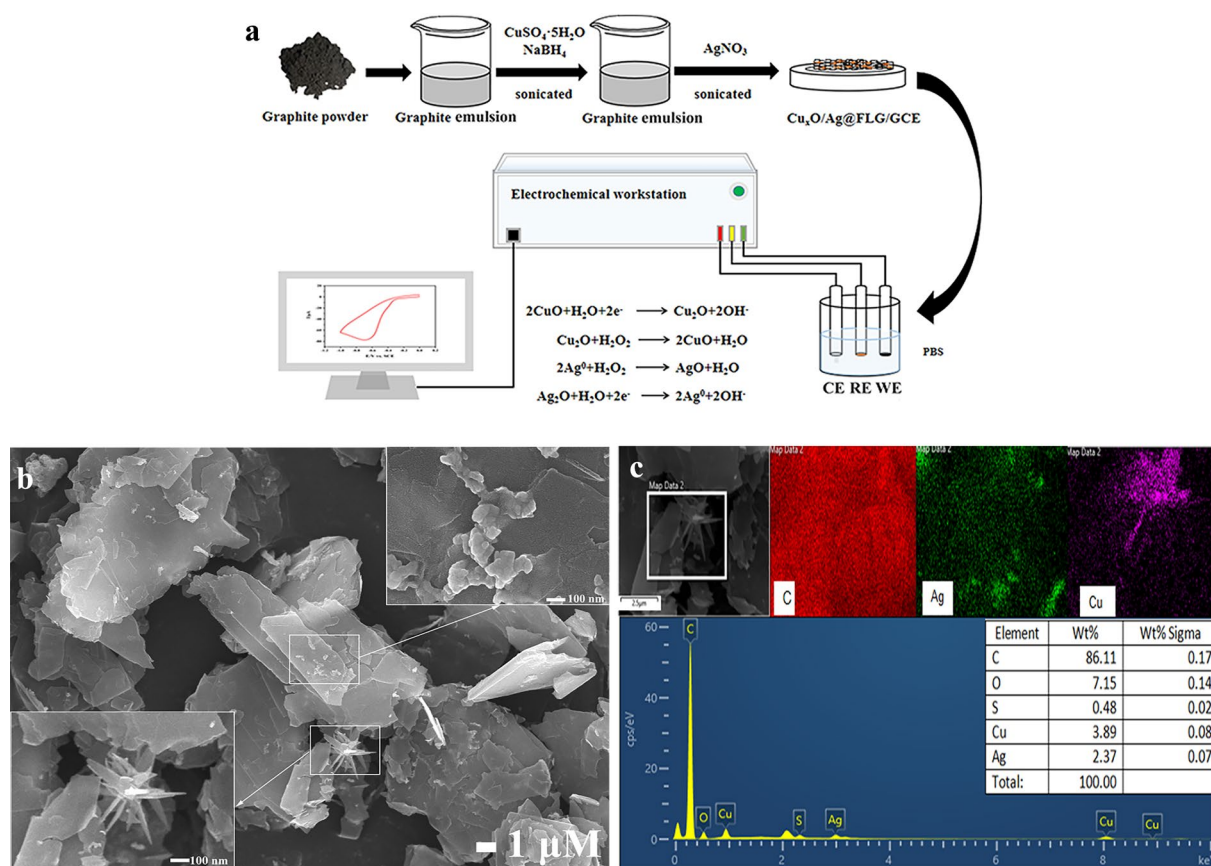


Figure 1. (a) preparation of $\text{Cu}_x\text{O}/\text{Ag}@/\text{FLG}$ and mechanism of detecting H_2O_2 , (b) SEM images and (c) EDS images of $\text{Cu}_x\text{O}/\text{Ag}@/\text{FLG}$.

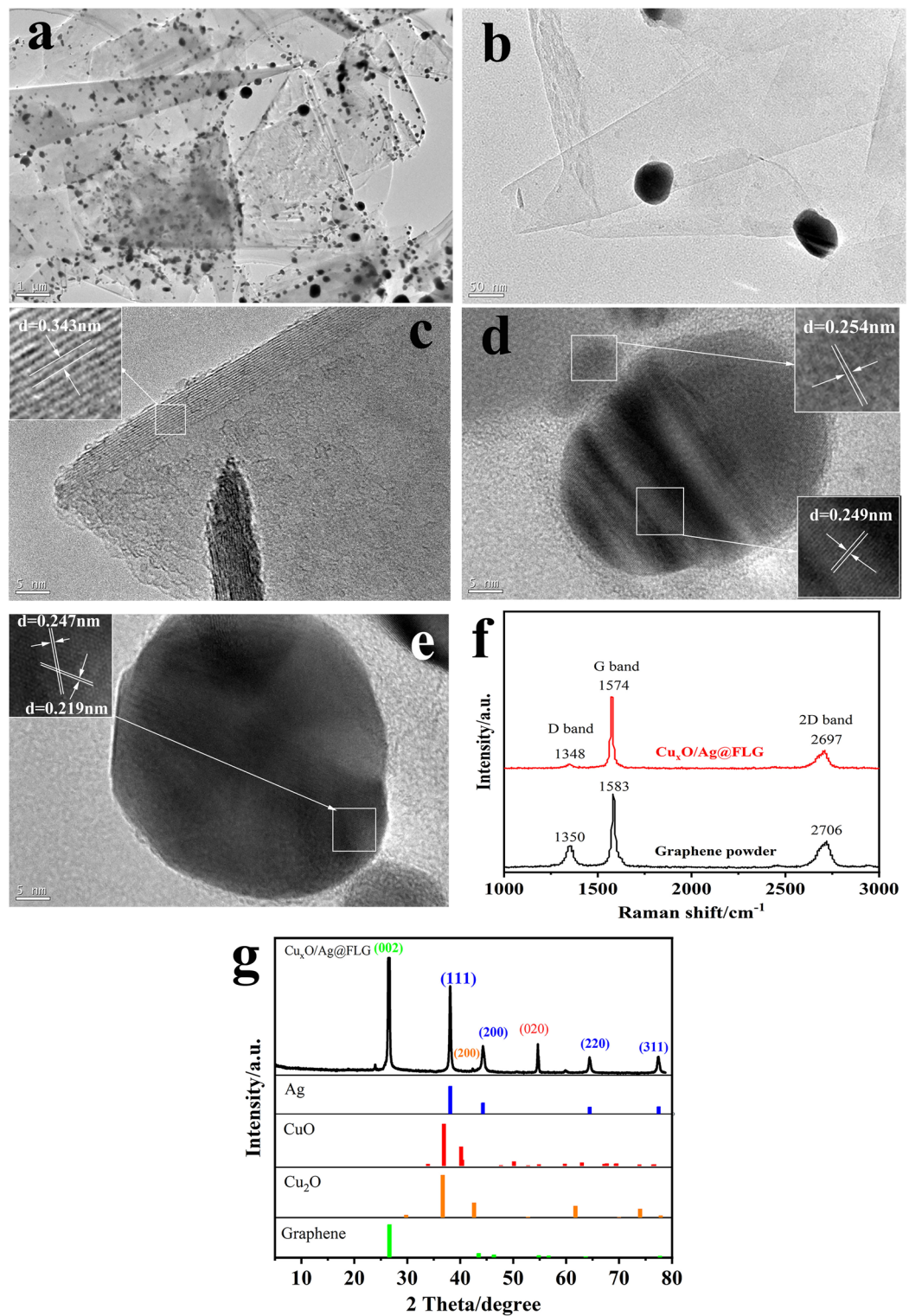


Figure 2. (a,b) TEM images, (c–e) high resolution TEM (HRTEM) images and (f) Raman spectra (g) XRD pattern of $\text{Cu}_x\text{O}/\text{Ag}@\text{FLG}$.

is the characteristic peak of graphene's (002) plane (JCPDS no. 41-1487). The peaks at 38.08° , 44.26° , 64.4° , and 77.46° can be assigned to (111), (200), (220) and (311) planes of Ag^0 (JCPDS no. 04-0783). Other peaks at 42.33° and 53.54° respectively arise from (200) plane of Cu_2O and (020) plane of CuO (JCPDS no. 74-1230 and JCPDS no. 45-0937).

Materials	D band	G band	2D band	2D FWHM	I _D /I _G	I _{2D} /I _G
Graphite powder	1350	1583	2706	84.83	0.626	1.122
Cu _x O/Ag@FLG	1348	1574	2697	81.15	0.204	4.779

Table 1. The Raman fitting data of graphite powder and Cu_xO/Ag@FLG.

Characterizations of element binding states. Furthermore, the element composition and valence states of elements Cu_xO/Ag@FLG nanocomposites were analyzed by XPS. The full scan XPS spectra of Cu_xO/Ag@FLG showed signals corresponding to C 1s, O 1s, Cu 2p and Ag 3d (Fig. 3a). As exhibited in Fig. 3b, the peaks at 284.3, 285.4, 286.65 and 289.5 eV are attributed to C–C/C=C, C–O, C=O and O–C=O species. Compared to graphene oxide, the above C 1s XPS spectrum is more similar to reduced graphene oxide, because the peak intensity for C–C are significantly stronger than C–O and C=O²³. Figure 3c indicated that the characteristic peaks at 531.6 eV, 532.5 eV which belong to lattice oxygen of Cu₂O and CuO²⁴, respectively, and the peaks at 533.5 eV, 530.3 eV are usually attributed to O in adsorbed –OH groups or carbonates²⁵. The Cu 2p spectrum (Fig. 3d) was deconvoluted into seven peaks. The peaks at the binding energy of 933.35 eV of Cu 2p_{3/2} and 953.6 eV of Cu 2p_{1/2} are consistent with the representative spin–orbit of Cu⁺. At the same time, the peaks at the binding energy of 934.8 eV of Cu 2p_{3/2} and 954.9 eV of Cu 2p_{1/2} are characteristic peaks for Cu²⁺²⁶. The peaks at 942.2, 944.8 and 963.1 eV are correspond to satellite peaks of Cu 2p in CuO²⁷. The Ag 3d spectrum (Fig. 3e) was deconvoluted into two peaks, the peak of Ag 3d_{5/2} at 368.6 eV and the peak of Ag 3d_{3/2} at 374.6 eV are attributed to Ag⁰²⁸.

Electrochemical characterizations of the modified electrodes. As depicted in Fig. 4, the interfacial characteristics of the modified electrodes were investigated by EIS. Generally, the diameter semicircle at high frequency represents the resistance to charge transfer (Rct)²⁹. In Fig. 4a, compared with the Rct of bare GCE (5774 Ω), the Rct increases to 12,154 Ω after modified with Cu_xO@FLG by reason of weak conductivity of Cu₂O and CuO. However, the Rct decreases to 2464 Ω when modified with Ag@FLG, which indicates that Ag@FLG can promote electron transfer greatly. Furthermore, it is worth noting that Cu_xO/Ag@FLG/GCE has the smallest Rct (1605 Ω), which illustrates its excellent electron transport ability owing to the large surface area and the potential synergism of the nanocomposites. Figure 4b further confirms the above inference peak-to-peak separation (ΔE_p) of GCE, Cu_xO@FLG/GCE, Ag@FLG/GCE and Cu_xO/Ag@FLG/GCE are 265, 332, 429 and 221 mV respectively, indicating Cu_xO/Ag@FLG can promote the electron transfer on the electrode surface to the most extent. The peak current of Cu_xO/Ag@FLG/GCE is the largest, which is 3.98 times of GCE, 2.58 times of Cu_xO@FLG/GCE and 1.55 times of Ag@FLG/GCE. It is clear that Ag@FLG/GCE has a larger peak current of redox peaks of [Fe(CN)₆]^{3-/4-} couple, suggesting that the electrochemical probe of [Fe(CN)₆]^{3-/4-} has good electron transfer at Ag@FLG/GCE due to its excellent electronic conductivity. However, on Cu_xO@FLG/GCE, the redox peak current of [Fe(CN)₆]^{3-/4-} are much smaller, suggesting that the material of Cu_xO@FLG is less effective for the electron transfer of the [Fe(CN)₆]^{3-/4-} because of its inferior conductivity. It is interesting that when the Cu_xO/Ag@FLG/GCE electrode was applied, the redox peak current was enhanced much more comparison with Ag@FLG, showing that the Cu_xO/Ag@FLG/GCE nanocomposite has better performance for electron transfer of electrochemical probe than the single-component of Ag@FLG or Cu_xO@FLG. Comparison histograms of Rct, ΔE_p and peak current (I_p) of different electrodes are shown in Fig. 4c.

Electrochemical detection of H₂O₂. Electrochemical reduction of H₂O₂ by the synthesized composite was studied using CV method. Therefore, the CV curves are shown in Fig. 5 in N₂-saturated 0.01 M PBS contained 4 mM H₂O₂ at a scan rate of 50 mV s⁻¹. The reduction peak current enhancement of Cu_xO@FLG/GCE is extremely weak (Fig. 5a). In addition, Ag@FLG show higher current response thanks to exceptional electrocatalytic activity of Ag NPs. CV curve of Cu_xO/Ag@FLG/GCE has shown a lower reduction potential at –0.65 V and higher current of 80 μA. Therefore, the Cu_xO/Ag@FLG/GCE is a prospective electrochemical sensor for H₂O₂ detection. With the increase of H₂O₂ addition, the cathodic current increases linearly in Fig. 5b. Subsequently, the CV curves of Cu_xO/Ag@FLG at varying scan rates (10–120 mV s⁻¹) in 0.01 M PBS (pH 7.4) contained 4 mM H₂O₂ were investigated (Fig. 5c). Along with the square root of the scanning speed, the reduction peak current increases linearly, and correlation coefficients (R²) was fitted as 0.9803, which indicates that the diffusion-controlled electrochemical process (Fig. 5d,e)³⁰.

Mechanism for electrocatalytic reduction. The reaction mechanism of H₂O₂ electrocatalytic reduction of Cu_xO/Ag@FLG nanocomposites is illustrated in the following chemical formula reduction. Primarily, CuO reduced to Cu₂O, and Cu₂O of the composite and that be reduced reacted with H₂O₂ to form CuO and H₂O. Equations (1) and (2) can convey the reduction of H₂O₂ by Cu_xO on Cu_xO/Ag@FLG composite. Besides, Ag⁰ of Cu_xO/Ag@FLG composite was oxidated to Ag₂O with H₂O₂ was restored to H₂O. Equations 3 can represent the reduction of H₂O₂ by Ag⁰ on Cu_xO/Ag@FLG composite.



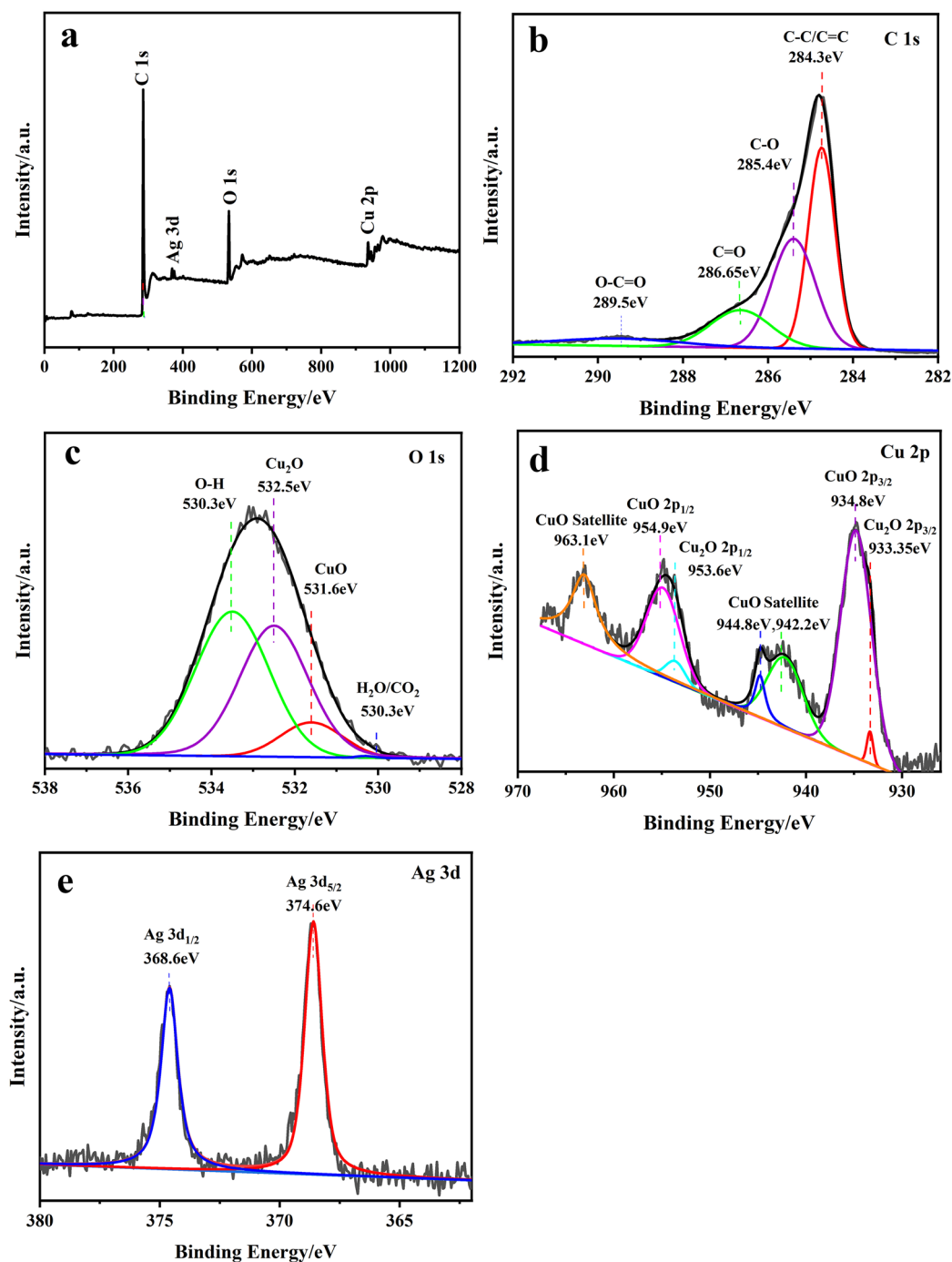


Figure 3. XPS spectra of $\text{Cu}_x\text{O}/\text{Ag}@FLG$: (a) full survey spectrum. High-resolution spectra of (b) C 1s, (c) O 1s, (d) Cu 2p, and (e) Ag 3d, respectively.



Amperometric detection of H_2O_2 at $\text{Cu}_x\text{O}/\text{Ag}@FLG/\text{GCE}$. Then, the parameters for detecting H_2O_2 were optimized which include volume of catalyst ink, pH of supporting electrolyte and applied potential. The response current is the largest when the volume of ink was 5 μL (Fig. 6a). Furthermore, volume of 5 μL $\text{Cu}_x\text{O}/\text{Ag}@FLG$ composite on GCE is used for further studies. As shown in the Fig. 6b, CV curves was tested in PBS with different pH containing 4 mM H_2O_2 , as a result, the maximum current response appears in PBS with pH

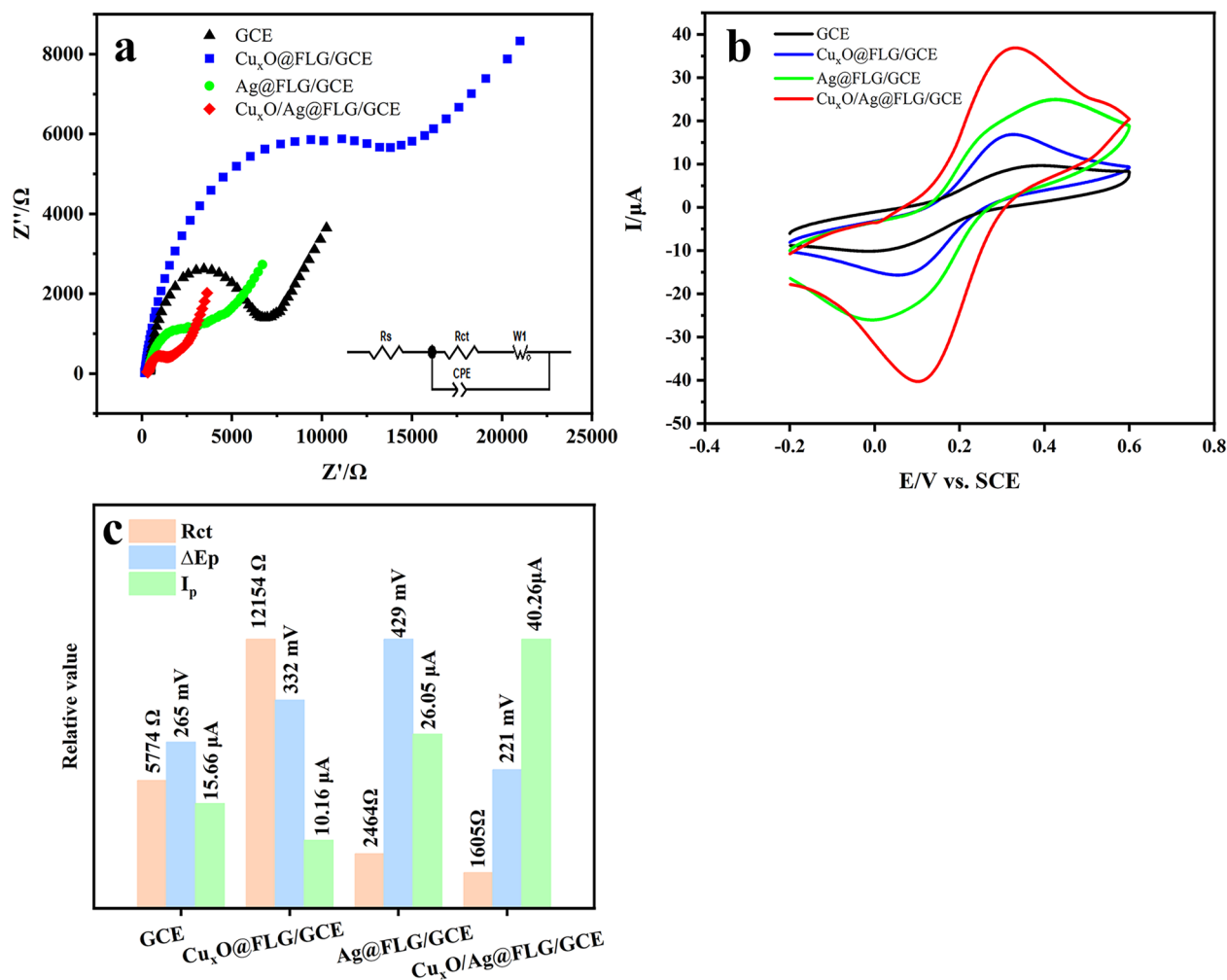


Figure 4. (a) EIS of bare GCE, Cu_xO@FLG/GCE, Ag@FLG/GCE, Cu_xO/Ag@FLG/GCE in 1 mM K₃[Fe(CN)₆]/1 mM K₄[Fe(CN)₆]/100 mM KCl solution 10⁻¹–10⁵ Hz. The equivalent circuit is inserted; (b) CV of bare GCE, Cu_xO@FLG/GCE, Ag@FLG/GCE, Cu_xO/Ag@FLG/GCE in 1 mM K₃[Fe(CN)₆]/1 mM K₄[Fe(CN)₆]/100 mM KCl solution at a scanning speed of 50 mV·s⁻¹; (c) the histogram of R_{ct}, ΔE_p and I_p of different electrodes.

7.4. Therefore, PBS with pH 7.4 was selected as the electrolyte solution. The influence of different applied potentials on sensitivity was investigated by *i*-*t* method (Fig. 6c). The sensitivity was the highest at -0.65 V. Hence, -0.65 V is selected as the detection potential in the following studies.

Under the best conditions (5 μL Cu_xO/Ag@FLG ink, 0.01 PBS with pH 7.4, -0.65 V), *i*-*t* curve was plotted for Cu_xO/Ag@FLG/GCE as H₂O₂ was added every 40 s (Fig. 7a). The response time of Cu_xO/Ag@FLG/GCE to H₂O₂ is about 5 s. Meanwhile, the linear relationship between concentration of H₂O₂ and current is fitted (Fig. 7b), the current increases linearly with increasing concentration in the range of 10–100,000 μM, the linear equation is $I (\mu\text{A}) = -12.330 c (c \text{ is the concentration of H}_2\text{O}_2, \text{ mM}) - 13.963$, $R^2 = 0.9978$, the detection limit is 2.13 μM ($S/N = 3$), and the sensitivity is 174.5 μA mM⁻¹ cm⁻². These are attributed to the large specific surface area of graphene sheet and the synergistic effect of graphene, Cu_xO and Ag NPs in reducing H₂O₂ and amplifying signal.

Figure 8a demonstrates the *i*-*t* curve of the Cu_xO/Ag@FLG/GCE sensor after addition of 1 mM H₂O₂, 1 mM Val, DA, AA, UA, CA, LA, Gly, Arg, Lys, Glu, CaCl₂, MgCl₂, NaCl, FeCl₃, and a second injection 1 mM H₂O₂. After adding interferent, the current response to H₂O₂ on Cu_xO/Ag@FLG/GCE at the detection potential is very small, which indicates that the response of the sensor to H₂O₂ is almost not affected in the presence of other compounds, Cu_xO/Ag@FLG/GCE shows high selectivity. Long-term stability and reproducibility are momentous factors which evaluate the performance of sensors. Five Cu_xO/Ag@FLG/GCE electrodes were prepared respectively, and the relative standard deviation (RSD) of current response in the same concentration of H₂O₂ was 3.69%, which presents a good repeatability (Fig. 8b). After storing at room temperature for 1 month, the reaction of the prepared electrode to H₂O₂ decreased to about 95% (Fig. 8c), which illustrates that it has long-term stability. In a word, our research makes it clear that Cu_xO/Ag@FLG/GCE is reliable as an electrochemical sensor of H₂O₂. At the same time, it has the potentiality to detect H₂O₂ in real samples in complex environment.

The comparison of Cu_xO/Ag@FLG/GCE sensor with other H₂O₂ sensors containing CuO, Cu₂O and Ag is listed in Table 2. Significantly, as-synthesized sensor in this study has a wider detection range and a lower detection limit. Compared with other reported electrochemical sensors for H₂O₂ detection, the Cu_xO/Ag@FLG/GCE

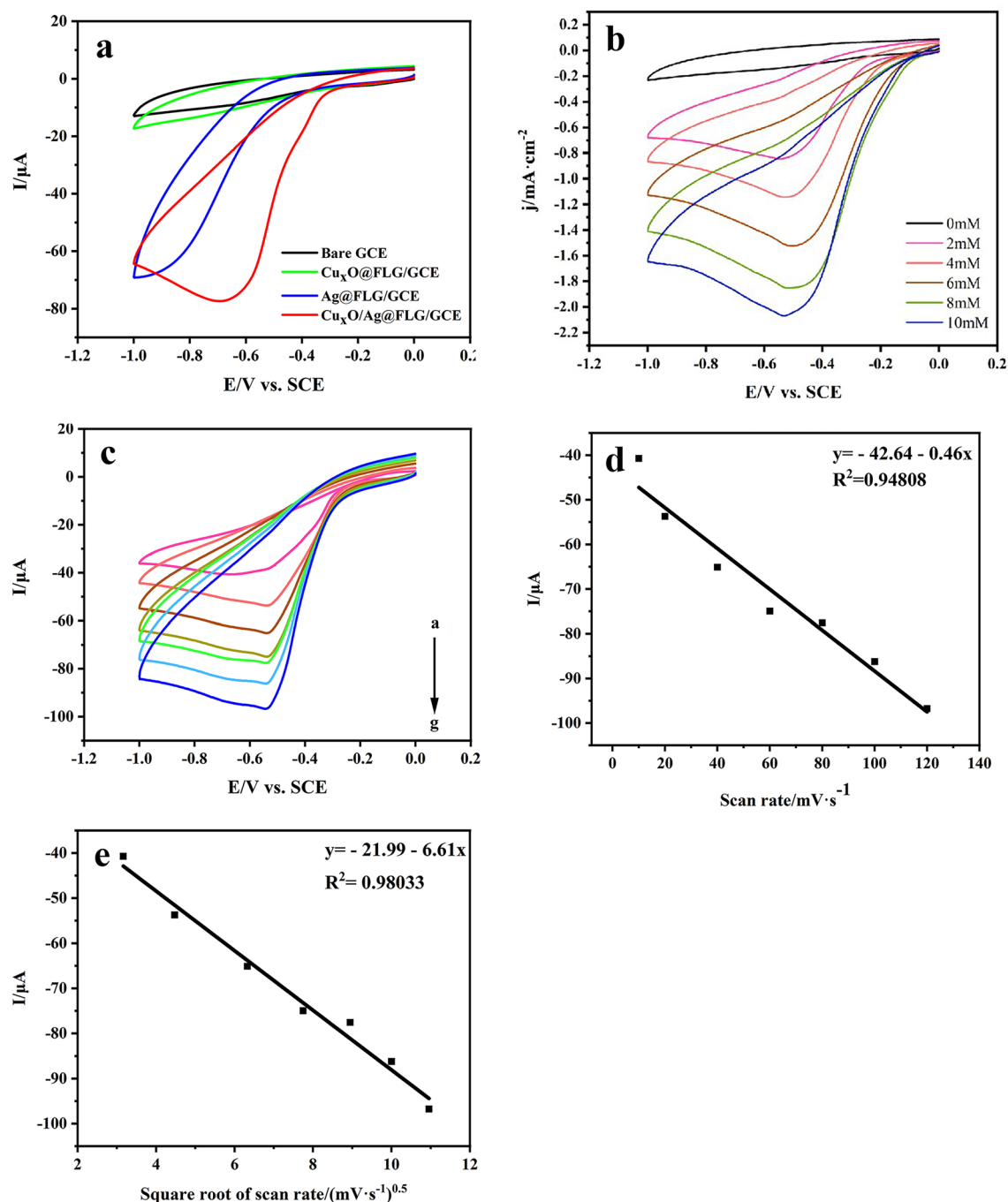


Figure 5. (a) CV of bare GCE, $\text{Cu}_x\text{O@FLG/GCE}$, Ag@FLG/GCE , $\text{Cu}_x\text{O/Ag@FLG/GCE}$ in the presence of 4 mM H_2O_2 ; (b) CV curves of $\text{Cu}_x\text{O/Ag@FLG/GCE}$ in the presence of 0, 2, 4, 6, 8, 10 mM H_2O_2 ; (c) CV curves of $\text{Cu}_x\text{O/Ag@FLG/GCE}$ in the presence of 4 mM H_2O_2 at various scan rates; plots of cathodic peak current (I_p) vs. (d) root of scan rate or (E) square root of scan rate ($v^{1/2}$).

electrode has a significant advantage in terms of reaction time and sensitivity. Furthermore, the production and application of the obtained $\text{Cu}_x\text{O/Ag@FLG/GCE}$ electrode are inexpensive, simple and easy to control, resulting in a potential perspective for convenient, fast, sensitive and cost-effective detection of H_2O_2 .

Detection of H_2O_2 in milk sample. In addition, the H_2O_2 concentration in milk samples were determined to further evaluate the availability and practical application of the $\text{Cu}_x\text{O/Ag@FLG/GCE}$. To reduce the sample matrix effect, milk from two different brands was centrifuged for 15 min at 7,000 rpm, then diluted 10 times with deionized water and filtered with 0.22 μm microporous membrane filtration to obtain milk solution. Finally, the obtained recovery of H_2O_2 was calculated using the standard addition method. Amperometric curve

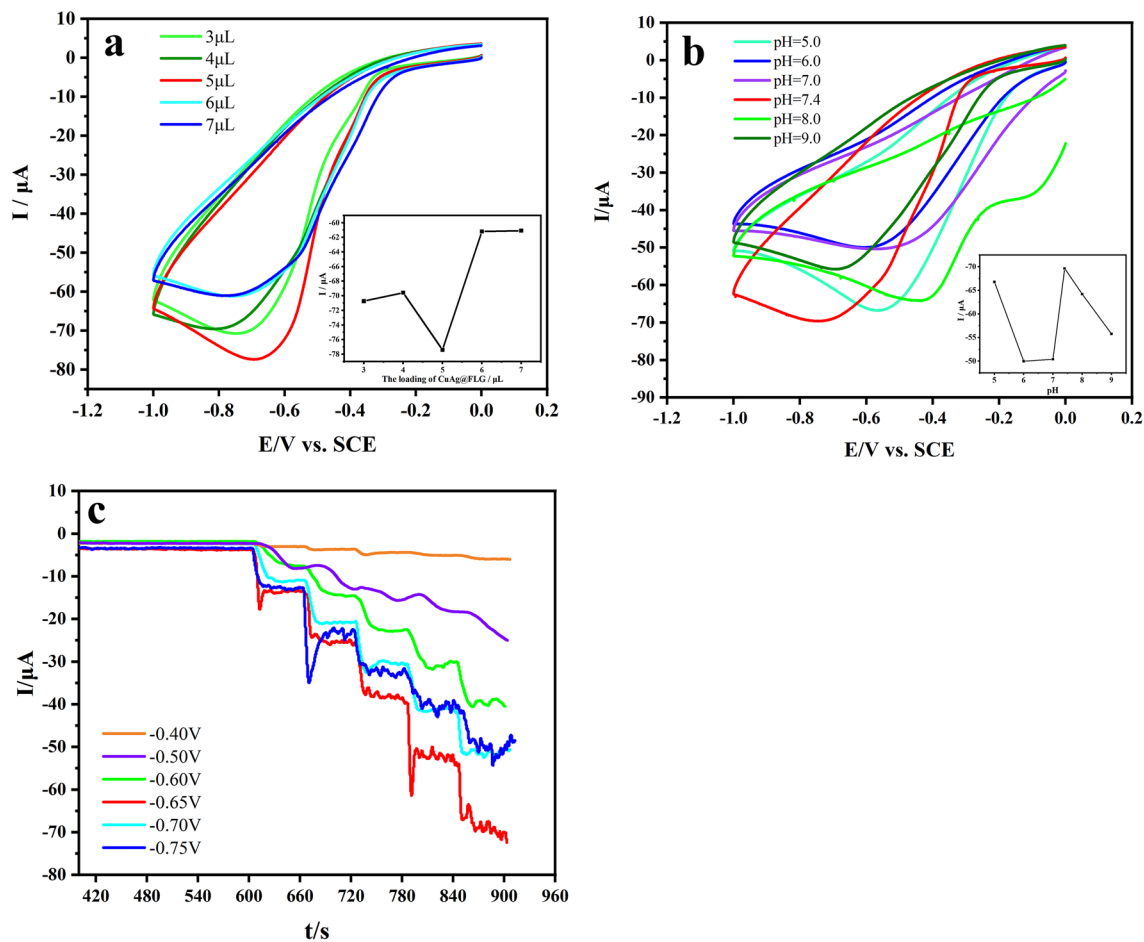


Figure 6. CVs at a scan rate of 0.05 V s^{-1} of $\text{Cu}_x\text{O}/\text{Ag}@FLG/\text{GCE}$ (a) with different volume of $\text{Cu}_x\text{O}/\text{Ag}@FLG$ in 0.01 M PBS (pH 7.4) containing 4.0 mM H_2O_2 ; (b) in PBS with different pH include 5.0, 6.0, 7.0, 7.4, 8.0, 9.0 containing 4 mM H_2O_2 . (c) I-t curves of $\text{Cu}_x\text{O}/\text{Ag}@FLG/\text{GCE}$ at applied potentials with successive addition of H_2O_2 into 0.01 M PBS.

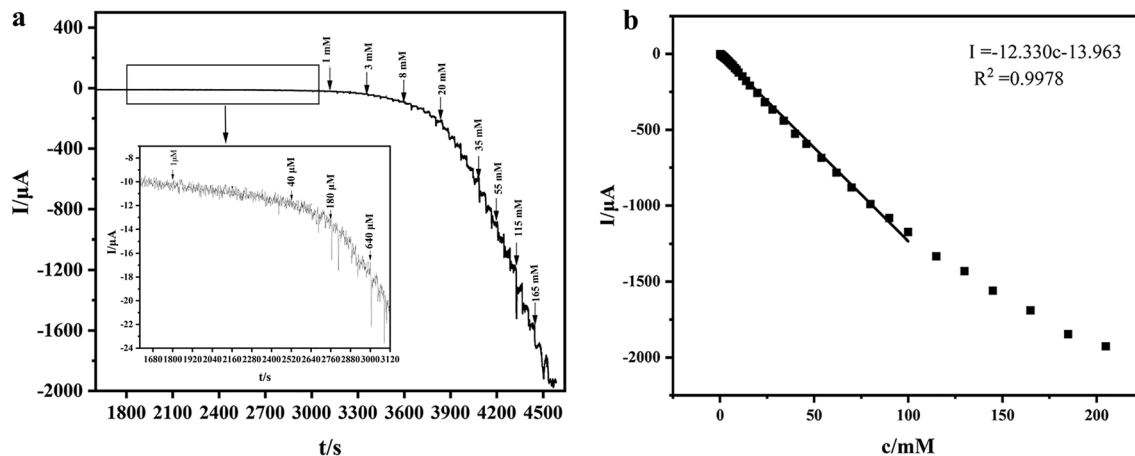


Figure 7. (a) I-t curve of the $\text{Cu}_x\text{O}/\text{Ag}@FLG/\text{GCE}$ for consecutive additions of H_2O_2 at -0.65 V . The illustration shows the enlarged i-t curve in the low concentration area; (b) corresponding fitting curve.

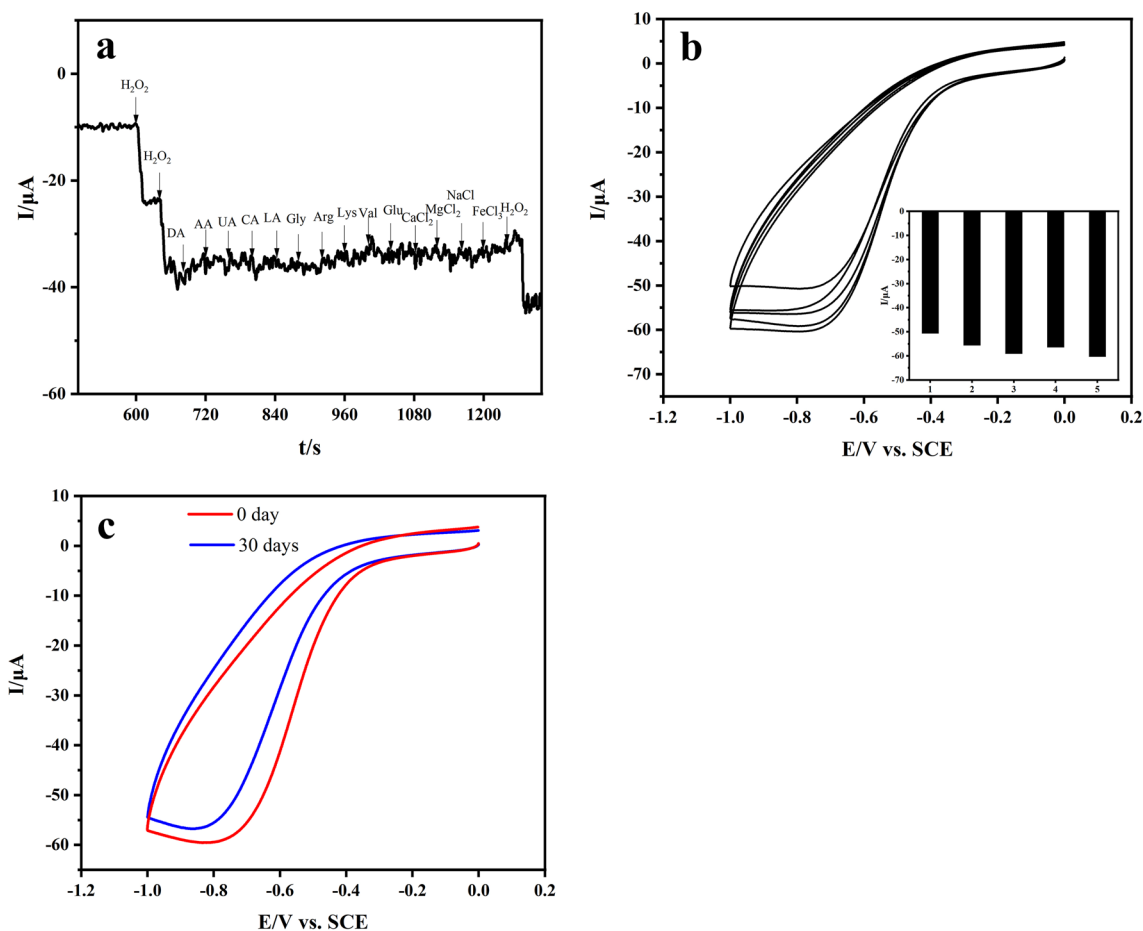


Figure 8. (a) Amperometric response recorded at $\text{Cu}_x\text{O}/\text{Ag}@FLG/\text{GCE}$ in 0.01 M PBS with the additions of H_2O_2 (1 mM), DA, AA, LA, Gly, UA, Arg, Lys, CA, Val, Glu, CaCl_2 , MgCl_2 , NaCl, FeCl_3 ; (b) CV curves of $\text{Cu}_x\text{O}/\text{Ag}@FLG/\text{GCE}$ in 0.01 M PBS contained 4 mM H_2O_2 at five equally prepared $\text{Cu}_x\text{O}/\text{Ag}@FLG/\text{GCE}$ sensors; (c) CV curves of the $\text{Cu}_x\text{O}/\text{Ag}@FLG/\text{GCE}$ in PBS contained 4 mM H_2O_2 tested at 1st day and 30th day.

Modified material	Detection limit (μM)	Linear range (μM)	Sensitivity ($\mu\text{A } \mu\text{M}^{-1} \text{cm}^{-2}$)	References
$\text{CuO}/\text{g-C}_3\text{N}_4/\text{GCE}$	0.31	0.5–50	3.327	31
$\text{CuO-SWCNT-PDDA}/\text{GCE}$	20.8	300–7800	4.396	32
$\text{Cu}_2\text{O-rGO}$	21.7	30–12,800	0.0195	33
$\text{Cu}_2\text{O}/\text{TiO}_2/\text{Ti}$	90.5	500–8000	0.412	34
$\text{CQDs}/\text{octahedral } \text{Cu}_2\text{O}/\text{GCE}$	8.4	20–4300	0.000298	35
$\text{Ag NPs}/3\text{DG}/\text{GCE}$	14.9	30–16,210	1.094	36
$\text{Ag NPs}/\text{N-G}/\text{GCE}$	1.2	100–126,400	0.0446	37
$\text{Ag}/\text{Cu}_2\text{O}/\text{ITO}$	0.1	500–30,000	0.0502	38
$\text{Cu}_x\text{O}/\text{Ag}@FLG/\text{GCE}$	2.13	10–100,000	0.1745	This work

Table 2. Comparison of H_2O_2 sensors related to CuO , Cu_2O and Ag in different literature.

was detected at -0.65 V under successive adding the milk sample, which were displayed in Fig S1. As shown in Table 3, the recovery for H_2O_2 in the sample was 90.12–102.00%.

Conclusions

To summaries, $\text{Cu}_x\text{O}/\text{Ag}@FLG$ sensor has been prepared successfully by ultrasonic exfoliation method. $\text{Cu}_x\text{O}/\text{Ag}@FLG/\text{GCE}$ electrode has shown excellent catalytic reduction performance for H_2O_2 , such as wide linearity range (10–100,000 μM), low detection limit (2.13 μM), high sensitivity (174.5 $\mu\text{A } \text{mM}^{-1} \text{cm}^{-2}$) and long-term stability. In addition, the prepared sensor can detect H_2O_2 in milk samples, which makes it possible for quality control in food industry, suggesting that as-synthetic $\text{Cu}_x\text{O}/\text{Ag}@FLG$ has a broad application prospect in electrochemical sensors.

Real sample	Added (mM)	Found (mM)	Recovery (%)	Titrimetric method (mM)
Milk 1	0.050	0.051	102.00	0.053
	0.175	0.167	95.56	0.165
	0.425	0.383	90.12	0.432
Milk 2	0.050	0.048	96.00	0.056
	0.175	0.172	98.29	0.184
	0.425	0.401	94.35	0.384

Table 3. Actual sample analysis of $\text{Cu}_2\text{O}/\text{Ag}@\text{FLG}/\text{GCE}$ in milk ($n = 3$).

Data availability

The datasets generated during and/or analysed during the current study are available from the corresponding author on reasonable request.

Received: 11 December 2022; Accepted: 17 April 2023

Published online: 24 April 2023

References

- Salazar, P., Fernandez, I., Rodríguez, M. C., Hernandez-Creus, A. & González-Mora, J. L. One-step green synthesis of silver nanoparticle-modified reduced graphene oxide nanocomposite for H_2O_2 sensing applications. *J. Electroanal. Chem.* **855**, 113638 (2019).
- Yamamoto, K. *et al.* Highly-sensitive flow injection determination of hydrogen peroxide with a peroxidase-immobilized electrode and its application to clinical chemistry. *Anal. Chim. Acta* **406**(2), 201–207 (2000).
- Balu, S., Palanisamy, S., Velusamy, V. & Yang, T. C. Sonochemical synthesis of gum guar biopolymer stabilized copper oxide on exfoliated graphite: application for enhanced electrochemical detection of H_2O_2 in milk and pharmaceutical samples. *Ultrason. Sonochem.* **56**, 254–263 (2019).
- Song, S. *et al.* Peroxidase mimetic activity of Fe_3O_4 nanoparticle prepared based on magnetic hydrogels for hydrogen peroxide and glucose detection. *J. Colloid Interface Sci.* **506**, 46–57 (2017).
- Salazar, P., Rico, V. & González-Elipé, A. R. Non-enzymatic hydrogen peroxide detection at NiO nanoporous thin film-electrodes prepared by physical vapor deposition at oblique angles. *Electrochim. Acta* **235**, 534–542 (2017).
- Thatikayala, D. *et al.* Progress of advanced nanomaterials in the non-enzymatic electrochemical sensing of glucose and H_2O_2 . *Biosensors* **10**(11), 151 (2020).
- Wang, M. *et al.* A novel H_2O_2 electrochemical sensor based on NiCo_2S_4 functionalized reduced graphene oxide. *J. Alloy. Compd.* **784**, 827–833 (2019).
- Jiang, L. C. & Zhang, W. D. Electrodeposition of TiO_2 nanoparticles on multiwalled carbon nanotube arrays for hydrogen peroxide sensing. *Electroanal. Int. J. Devoted Fundam. Pract. Aspects Electroanal.* **21**(8), 988–993 (2009).
- Hwang, E. T. & Gu, M. B. Enzyme stabilization by nano/microsized hybrid materials. *Eng. Life Sci.* **13**(1), 49–61 (2013).
- Manavalan, S., Ganesamurthi, J., Chen, S.-M., Veerakumar, P. & Murugan, K. A robust $\text{Mn@FeNi-S}/\text{graphene oxide}$ nanocomposite as a high-efficiency catalyst for the non-enzymatic electrochemical detection of hydrogen peroxide. *Nanoscale* **12**(10), 5961–5972 (2020).
- Agrisuelas, J., González-Sánchez, M.-I. & Valero, E. Hydrogen peroxide sensor based on in situ grown Pt nanoparticles from waste screen-printed electrodes. *Sens. Actuators B Chem.* **249**, 499–505 (2017).
- Qin, X. *et al.* One-step synthesis of Ag nanoparticles-decorated reduced graphene oxide and their application for H_2O_2 detection. *Electrochim. Acta* **79**, 46–51 (2012).
- Tran, H. V., Le, T. A., Giang, B. L., Piro, B. & Dai Tran, L. Silver nanoparticles on graphene quantum dots as nanozyme for efficient H_2O_2 reduction in a glucose biosensor. *Mater. Res. Express.* **6**(11), 115403 (2019).
- Tran, H. V., Huynh, C. D., Tran, H. V. & Piro, B. Cyclic voltammetry, square wave voltammetry, electrochemical impedance spectroscopy and colorimetric method for hydrogen peroxide detection based on chitosan/silver nanocomposite. *Arab. J. Chem.* **11**(4), 453–459 (2018).
- Tran, H. V., Trinh, A. X., Huynh, C. D. & Le, H. Q. Facile hydrothermal synthesis of silver/chitosan nanocomposite and application in the electrochemical detection of hydrogen peroxide. *Sens. Lett.* **14**(1), 32–38 (2016).
- Dhara, K. & Mahapatra, D. R. Recent advances in electrochemical nonenzymatic hydrogen peroxide sensors based on nanomaterials: a review. *J. Mater. Sci.* **54**(19), 12319–12357 (2019).
- Yang, Z., Qi, C., Zheng, X. & Zheng, J. Synthesis of silver nanoparticle at a gas/liquid interface in the presence of silver seeds and its application for electrochemical sensing. *Talanta* **140**, 198–203 (2015).
- Manzetti, S., Vasilache, D. & Francesco, E. Emerging carbon-based nanosensor devices: structures, functions and applications. *Adv. Manuf.* **3**(1), 63–72 (2015).
- Zhang, Y. *et al.* Highly sensitive graphene–Pt nanocomposites amperometric biosensor and its application in living cell H_2O_2 detection. *Anal. Chem.* **86**(19), 9459–9465 (2014).
- Liu, G., Chen, J., Hou, X. & Huang, W. A highly-sensitive electrochemical sensor for the simultaneous detection of Cd^{2+} and Pb^{2+} using liquid phase-exfoliated graphene. *Anal. Methods* **6**(15), 5760–5765 (2014).
- Elfadil, D. *et al.* Liquid-phase exfoliated 2D graphene nanoflakes electrochemical sensor coupled to molecularly imprinted polymers for the determination of citrinin in food. *Talanta* **253**, 124010 (2023).
- Zhou, H. *et al.* Raman scattering of monolayer graphene: the temperature and oxygen doping effects. *J. Phys. D Appl. Phys.* **44**(18), 185404 (2011).
- She, Y., Lu, Z., Fan, W., Jewell, S. & Leung, M. K. Facile preparation of PdNi/rGO and its electrocatalytic performance towards formic acid oxidation. *J. Mater. Chem. A* **2**(11), 3894–3898 (2014).
- Johra, F. T. & Jung, W.-G. Low temperature synthesis of RGO-Au nanocomposite with apparently reduced time and its application as a chemical sensor. *Appl. Surf. Sci.* **362**, 169–175 (2016).
- Wang, T. *et al.* Controllable synthesis of hierarchical porous Fe_3O_4 particles mediated by poly (diallyldimethylammonium chloride) and their application in arsenic removal. *ACS Appl. Mater. Interfaces.* **5**(23), 12449–12459 (2013).
- Shen, H. *et al.* All-solid-state Z-scheme system of $\text{RGO-Cu}_2\text{O}/\text{Bi}_2\text{O}_3$ for tetracycline degradation under visible-light irradiation. *Chem. Eng. J.* **313**, 508–517 (2017).

27. Sabbe, P.-J. *et al.* Synthesis and surface characterization of a patterned cuprite sample: Preparatory step in the evaluation scheme of an X-ray-excited optical microscopy system. *Appl. Surf. Sci.* **332**, 657–664 (2015).
28. Li, D., Meng, L., Dang, S., Jiang, D. & Shi, W. Hydrogen peroxide sensing using Cu₂O nanocubes decorated by Ag–Au alloy nanoparticles. *J. Alloy. Compd.* **690**, 1–7 (2017).
29. Ciureanu, M. & Wang, H. Electrochemical impedance study of electrode-membrane assemblies in PEM fuel cells: I Electro-oxidation of H₂ and H₂/CO mixtures on Pt-based gas-diffusion electrodes. *J. Electrochem. Soc.* **146**(11), 4031 (1999).
30. Mani, V. *et al.* Core-shell heterostructured multiwalled carbon nanotubes@ reduced graphene oxide nanoribbons/chitosan, a robust nanobiocomposite for enzymatic biosensing of hydrogen peroxide and nitrite. *Sci. Rep.* **7**(1), 1–10 (2017).
31. Atacan, K. & Özacar, M. Construction of a non-enzymatic electrochemical sensor based on CuO/g-C₃N₄ composite for selective detection of hydrogen peroxide. *Mater. Chem. Phys.* **266**, 124527 (2021).
32. Liu, M., Liu, R. & Chen, W. Graphene wrapped Cu₂O nanocubes: non-enzymatic electrochemical sensors for the detection of glucose and hydrogen peroxide with enhanced stability. *Biosens. Bioelectron.* **45**, 206–212 (2013).
33. Xu, F., Deng, M., Li, G., Chen, S. & Wang, L. Electrochemical behavior of cuprous oxide-reduced graphene oxide nanocomposites and their application in nonenzymatic hydrogen peroxide sensing. *Electrochim. Acta* **88**, 59–65 (2013).
34. Wen, X., Long, M. & Tang, A. Flake-like Cu₂O on TiO₂ nanotubes array as an efficient nonenzymatic H₂O₂ biosensor. *J. Electroanal. Chem.* **785**, 33–39 (2017).
35. Li, Y., Zhong, Y., Zhang, Y., Weng, W. & Li, S. Carbon quantum dots/octahedral Cu₂O nanocomposites for non-enzymatic glucose and hydrogen peroxide amperometric sensor. *Sens. Actuators B Chem.* **206**, 735–743 (2015).
36. Zhan, B. *et al.* A hydrogen peroxide electrochemical sensor based on silver nanoparticles decorated three-dimensional graphene. *Appl. Phys. Lett.* **104**(24), 243704 (2014).
37. Tian, Y., Wang, F., Liu, Y., Pang, F. & Zhang, X. Green synthesis of silver nanoparticles on nitrogen-doped graphene for hydrogen peroxide detection. *Electrochim. Acta* **146**, 646–653 (2014).
38. Juang, F.-R. & Chern, W.-C. Octahedral Cu₂O nanoparticles decorated by silver catalyst for high sensitivity nonenzymatic H₂O₂ detection. *Mater. Sci. Semicond. Process.* **101**, 156–163 (2019).

Author contributions

J.S.: methodology, investigation, formal analysis, original draft; J.S., Y.W., C.Y. and Q.D.: research literatures, data curation; Y.C.: supervision; Z.Y.: conceptualization, supervision; Y.L.: supervision, review and editing. All authors reviewed the manuscript.

Funding

Open access funding provided by 2022 Guangdong University Students' Entrepreneurship Practice Training Project (202210573043).

Competing interests

The authors declare no competing interests.

Additional information

Supplementary Information The online version contains supplementary material available at <https://doi.org/10.1038/s41598-023-33661-7>.

Correspondence and requests for materials should be addressed to Y.C., Z.Y. or Y.L.

Reprints and permissions information is available at www.nature.com/reprints.

Publisher's note Springer Nature remains neutral with regard to jurisdictional claims in published maps and institutional affiliations.



Open Access This article is licensed under a Creative Commons Attribution 4.0 International License, which permits use, sharing, adaptation, distribution and reproduction in any medium or format, as long as you give appropriate credit to the original author(s) and the source, provide a link to the Creative Commons licence, and indicate if changes were made. The images or other third party material in this article are included in the article's Creative Commons licence, unless indicated otherwise in a credit line to the material. If material is not included in the article's Creative Commons licence and your intended use is not permitted by statutory regulation or exceeds the permitted use, you will need to obtain permission directly from the copyright holder. To view a copy of this licence, visit <http://creativecommons.org/licenses/by/4.0/>.

© The Author(s) 2023